Properties of LEDs for the Calibration of PMTs for the Daya Bay Project

By

Dragana Jusic

Thesis submitted to the faculty of the Virginia Polytechnic Institute and State University
in partial fulfillment of the requirements for the degree of

Master of Science

In

Physics

Jonathan Link

Mark Pitt

Leo Piilonen

12/08/08
Blacksburg, VA

Keywords: Calibration, LED, Spectrum, Fluorescence

Properties of LEDs for the Calibration of PMTs for the Daya Bay Project

Dragana Jusic

ABSTRACT

The flavor oscillations of neutrinos due to the mixing of mass eigenstates have been thoroughly studied in several experiments. One missing piece of the puzzle is the mixing angle θ_{13}, which is being searched for by the Daya Bay experiment. Currently, the experiment is still in construction mode.

Part of the experiment involves building effective detectors for atmospheric muons, resulting in accurate detection of antineutrinos from the source. To ensure accurate detection, we must effectively calibrate the PMTs with the use of carefully chosen and calibrated LEDs.

This thesis details the study of several LEDs measured in an attempt to determine the properties of the most likely source for our calibration efforts. I measured the spectra of the LEDs meant for use in calibration, along with several others for the purpose of comparison of spectrum width and to find the evidence of fluorescence in the LEDs.

Table of Contents

List of Figures:

Acknowledgments:
I would like to extend my sincere thanks to my advisor, Jonathan Link for his help and support throughout this endeavor. I could not have done this without his aid and guidance. I would also like to thank Debabrata Mohapatra for his help with the equipment and his thorough explanations of everything I came to him with. In addition, I would like to thank Daniel Baker for his work on the simulations, and for his programming expertise and help whenever I needed it.

A special thanks also to Leo Piilonen for his suggestions for improving the experiment, and Randy Heflin for his loan of his monochrometer, as well as explanations of the properties of LEDs, and various optics related questions.

I also wish to thank Mark Pitt for his loan of power sources, as well as Norman Morgan and Fred Mahone of the electronics shop for building us all we needed in a speedy manner.

I would also like to thank JoEllen Narron for her organizing skills, and aid in getting me any information I needed quickly.

Last but not least, I would like to thank Peter Johnson for his aid this summer. All programs were co-written with Peter, and I could not have done it without him.

Chapter 1: Introduction

1.1 History:

1.1.1 Discovery of Neutrinos:

The existence of neutrinos has been hypothesized since 1930, when Pauli tried to explain the reason behind the apparent lack of conservation of energy and momentum in certain radioactive decays[1]. Physical evidence of the neutrino was finally found in 1956 when Cowan and Raines discovered the electron neutrino[2]. In the following years, the muon neutrino was discovered in 1962[3] and the tau neutrino was discovered in 2000[4].

Originally, neutrinos were believed to be massless, but through the study of disappearance rates, this theory was eventually discarded. These studies go back to 1968, when the Homestake (or Davis) solar neutrino experiment[5], after many calculations and recalculations, showed a discrepancy between the rate of solar neutrino interactions theorized to be detected and the number that was actually seen. John Bahcall calculated the expected rate, while Davis set up a detector in a gold mine in South Dakota. Davis consistently measured about a third of Bahcall's expected neutrinos, and neither could find fault with their calculations or setup. This discrepancy, dubbed the "solar neutrino problem," plagued physicists for many years.

A beginning towards the answer showed itself in 1986 when Mikheyev and Smirnov[6], expanding on Wolfenstein's work[7], noted that when neutrinos propagate through matter, flavor oscillations can be modified. The presence of electrons in matter causes charged currents to flow and causes weak interactions of electron neutrinos which lead to changes in the energy levels of the propagation eigenstates of neutrinos. They hypothesized that neutrinos in matter have a different effective mass than neutrinos in vacuum because neutrino oscillations depend upon the squared mass difference of the neutrinos. They called this the MSW effect. At this time, there was no proof that neutrinos had mass, so this theory was the beginning of the idea of neutrino mass eigenstates.

In 1985, the Kamiokande-II[8] experiment measured muon neutrinos from the atmosphere, and again the number detected was not equal to the expectation. They found

about one half of the neutrinos expected. This was known as the atmospheric neutrino deficit.

1.1.2 Previous Experiments:

Finally, hard evidence of neutrino oscillations was discovered. The first experiment with evidence was Super-Kamiokande in 1998, which showed that fewer atmospheric muon neutrinos came through the earth than came from above the detector. The experiment's results were taken as evidence of muon neutrinos changing to tau neutrinos[9]. Then, in 2001 the SNO experiment[10] in Canada showed compelling evidence of oscillations in solar neutrinos. It wasn't limited to measuring only one flavor of neutrino, and was able to distinguish between the three. They discovered that about 35% of the incoming solar neutrinos were electron neutrinos, but the total flux of neutrinos matched the rate expected to be coming from the sun. Since then, a theory has been developed stating that flavor conversions between the neutrinos is due to neutrino oscillations, and new experiments are being created to measure the parameters that describe these oscillations.

The MINOS experiment[11], consisting of two detectors placed near and far from a neutrino source, began collecting data in 2005. It supported the parameters that were discovered in the Super-K experiment, and it came away with upper limits for Δm^2_{23} and $2\sin^2\theta_{23}$. The K2K[12] experiment tested the results of Super-Kamiokande by directing a neutrino beam from KEK (A research institute in Japan) to Kamiokande, and found matching oscillation parameters. The Chooz experiment[13] is a preface to the Daya Bay experiment, in that it measured an upper limit for θ_{13}, which we will try and improve upon. It was located underground, to use the earth as a muon shield, and it used a nuclear power plant as a source of electron antineutrinos, so that inverse beta decay could be used to observe neutrinos. Chooz was the experiment that measured the lowest limit on θ_{13} to date.

1.2 Theory of Neutrino Mixing:

The quarks composing matter are not independent from each other; a quantum mixing exists between them. Neutrinos are not quarks, but they follow the same model. Each of

the three flavors of neutrino (electron, muon, tau) is a mixture of three basis elements (ν_1, ν_2, ν_3), known as mass eigenstates, in that they are states of pure mass. The mixing angles θ_{12}, θ_{23} and θ_{13} give a measure of how deeply blended these basis elements are. For example, if the mixing angles are small, an electron neutrino might be composed almost entirely of ν_1. These angles also have a profound effect on neutrinos' behavior; neutrinos with small mixing angles are affected by the passage through matter much more than those with large mixing angles. Also, for a few years now we've known that neutrinos have mass and therefore they mix. This mixing exists because the mass eigenstates are not equal to the flavor eigenstates. That is, $\nu_1 \neq \nu_e$ and $m_1 \neq m_2 \neq m_3$ because if they were equal there would be no mixing.[14]

1.2.1 Mixing Matrix:

The way that the neutrino masses interact with neutrino flavors is described by the mixing matrix U_{MNSP}, named for Z. Maki, M. Nagakawa, S. Sakata and B. Pontecorvo[15]:

$$U_{MSNP} = \begin{pmatrix} C_{12}C_{13} & C_{13}S_{12} & S_{13}e^{-i\delta_{cp}} \\ (-S_{12}C_{23} - C_{12}S_{13}e^{i\delta_{cp}}S_{23}) & (C_{12}C_{23} - S_{12}S_{13}e^{i\delta_{cp}}S_{23}) & C_{13}S_{23} \\ (S_{12}S_{23} - C_{12}S_{13}e^{i\delta_{cp}}C_{23}) & (-C_{12}S_{23} - S_{12}S_{13}e^{i\delta_{cp}}C_{23}) & C_{13}C_{23} \end{pmatrix} \begin{pmatrix} e^{i\phi_1} & 0 & 0 \\ 0 & e^{i\phi_2} & 0 \\ 0 & 0 & 1 \end{pmatrix}$$

The components of this matrix are enumerated as follows: $C_{jk} = \cos\theta_{jk}$, $S_{jk} = \sin\theta_{jk}$, δ_{cp} is the CP phase angle, and φ_1 and φ_2 are Majorana phases. The oscillations are completely described by six the three missing angles θ_{12}, θ_{23}, θ_{13}, two independent mass squared differences Δm_{21}^2 and Δm_{23}^2, and one CP violating phase δ_{CP}.

1.2.2 Known Quantities:

From earlier experiments, we have values for 4 of the parameters of the independent neutrino mixing. We know the squared mass differences Δm_{21}^2 and Δm_{23}^2, the mixing angles θ_{12}, θ_{23}, and we have an upper limit for θ_{13}. We know that θ_{12} and θ_{23} are fairly large ($\sin^2\theta_{12}=.314$, $\sin^2\theta_{23}=.44$) and that $\Delta m_{13}^2 = 2.5*10^{-3}$ eV. We have only an upper limit on θ_{13}, which is the measure of ν_3 in ν_e. (The larger the angle, the higher the amount of ν_3). From Chooz we know that the upper limit of $\sin^2 2\theta_{13}<.17$, which means $\theta_{13}<10°$.[14]

1.2.3 Reason for Experiment:

Experiments are now focusing on θ_{13} because, aside from being important in its own right, it will influence the setup of future experiments. Theoretically, we need to know its value so that our knowledge of neutrino eigenstates oscillation will be complete. Experimentally, we can't do anything else until we have θ_{13}. The mixing matrix element which provides the information on the CP phase angle appears always in the combo $U_{e3}=\sin\theta_{13}e^{-\delta CP}$. If θ_{13} is zero, then it is not possible to probe leptonic CP violation in oscillation experiments, which is why we're searching for θ_{13} first. Given the known mixing angles θ_{12} and θ_{23}, which are both sizable, we thus need to know the value of θ_{13} to a sufficient precision in order to design the future generation of experiments to search for δ_{CP}. In addition, the size of θ_{13} influences the matter effect (MSW effect), which can be used to determine the mass hierarchy (order of masses). If $\sin^2 2\ \theta_{13}>.03$, then the design of future oscillation experiments is straightforward. If $\sin^2 2\ \theta_{13}<.03$, new experimental techniques and accelerator technologies are required to carry out the same sets of measurements.[14]

1.3 The Experiment:

1.3.1 Why $\sin^2 2\theta_{13}$:

Because of the importance of θ_{13}, the Daya Bay experiment is designed with a sensitivity of 0.01 at 90% confidence level. Experimentally, we are still missing $\theta_{13,}\ \delta_{CP}$ and the sign of Δm_{13}^2, so the purpose of Daya Bay is to measure or find a lower bound for θ_{13}. The study of $\sin^2 2\theta_{13}$ using reactors cleanly separates θ_{13} from CP violation and the effects of neutrino propagation in the earth, playing an important role in resolving the neutrino-mass hierarchy and future measurements of CP violation in the lepton sector. A reactor-based determination of $\sin^2 2\theta_{13}$ will provide important, complementary info to that from long-baseline, accelerator-based experiments. The choice of $\sin^2 2\theta_{13}$ is based on the equation for the survival probability of ν_e to ν_e at baselines of a few kilometers and reactor energies given by:

$$P_{sur} = 1 - \sin^{2(}2\theta_{13})\sin 2(\Delta m_{13}^2 L/4E)$$

The first sine term is a constant which gives the amplitude of oscillation, and the second sine term gives the periodicity. So to find the probability of a flavor change, we need to know the sine term with the mixing angle. [14]

1.3.2 Experimental Layout and Reasoning:

We plan on running the experiment in an ideal part of China. In Daya Bay, there are already two nuclear power plants in operation, with a third that is set to come online in three years. Each plant consists of two reactor cores that are being used to produce electricity, and will be used in our experiment as the source of antineutrinos. The basic layout consists of two reactor plants separated by 1.1 km, with a third being built about 400m east of the easternmost one. They are roughly built in a straight line. Within each power plant, there are two pairs of reactor cores held at a distance of about 88m from each other. Each core produces 2.9 GW of thermal energy, releasing around 5.8×10^{20} antineutrinos per second with energies up to 8 MeV. However, about 75% of these have energies below 1.8 MeV, which is the threshold of the inverse beta decay reaction. That still leaves us with an abundance of antineutrinos to detect.[14]

The plants are located next to mountainous terrain, which will be used to block out the cosmic ray muons, so there will be less background noise within the detectors. In fact, the mountains provide enough cover to reduce the muon induced background to less than 1% of our detected antineutrino signal.[14]

There are three experimental halls, one far and two near, linked by tunnels. At each hall there is a set of detectors, two at the near ends and four at the far end. Ideally, the near detectors would be the same distance from the reactor cores, but they vary by several meters to optimize for experimental sensitivity (to allow for more muon coverage). The far hall is about 1.5km away from the two near sites. To maximize sensitivity, detectors are deployed in the far hall close to the 1^{st} oscillation maximum ($\Delta m^2 L/E = \pi/2$).

The first oscillation maximum happens at around 1800m from the source. The far site is actually 1985m from the Daya Bay cores and 1615m from the Ling Ao-Ling Ao II cores. Ideally, it would be equidistant from each, but at this position the coverage of the mountain is much bigger, allowing for a greater buffer between the detectors and incoming cosmic ray muons.[14]

1.3.3 Setup of Detectors:

The detectors are cylindrical, and are contained within a stainless steel tank. They are shielded by 2.5m of water to protect them from radioactivity and spallation neutrons from the surrounding rock. They consist of three cylindrical zones, each used for a different purpose. The innermost zone consists of 20 tons of liquid scintillator doped with 0.1% of gadolinium (Gd). This zone is used for the detection of antineutrinos by using the fact that a neutrino event is defined by the prompt positron signal and delayed neutron – capture signal, with each having specific timing and energy. The liquid scintillator is the target for the inverse beta decay reactions because of its hydrogen content, while the Gd has a very large neutron-capture cross-section and is vital in creating the delayed coincidence tag between prompt positrons and delayed neutrons. The second zone is filled with undoped liquid scintillator, and this zone is used to capture gamma rays that escape from the target, thus improving the efficiency of antineutrino detection. The third zone is filled with mineral oil and acts as a gamma attenuator for rays from radioactivity in the Photomultiplier Tubes (PMTs) and the tank itself. The PMTs are within this zone, there are 192 of them lining the walls, meant to be used to measure the visible light produced in the scintillator.[14]

Because we wish to achieve high sensitivities with this experiment, we also have to ensure that our data isn't corrupted by other events, such as incoming cosmic ray muons. The thickness of the mountain acts as a good buffer, but the remaining muons still need to be accounted for. We account for them by using a muon detector which consists of two parts. The first muon detector is the water buffer, instrumented with Photomultiplier Tubes and serves as a Cerenkov detector.

The outer region of the water pool is segmented into two zones bounded by white Tyvek sheets. PMTs are placed throughout the water pool to collect Cerenkov photons produced by cosmic ray muons. Above the pool the muon tracking detector is made of light-weight resistive-plate chambers. The anti-neutrino detector modules are submerged in the water pool which shields the modules from ambient radiation and untagged spallation neutrons.[14]

Chapter 2: Muon System

2.1 Background noise due to cosmic muons

As stated, the experiment consists of cylindrical anti-neutrino detectors submerged in water. The targets are only meant to detect anti-neutrinos, therefore a way is needed to cancel out the noise from other sources. The steps taken to identify and dismiss the outside noise are a vital part of the experiment. One major background is composed of muons traveling through matter and interacting with the particles available.

The antineutrino detector is designed to measure a certain event that shows the presence of an antineutrino. This event is the inverse beta decay reaction, therefore the detector need to be able to measure a positron and a neutron-capture signal in a certain time-frame.[14]

2.1.1 Sources of Background Noise:

Background events can occur due to either one source or two. If one source causes two reactions that meet the signal event criteria, then this is considered a correlated event. If two sources cause two events in the right time frame, then this is considered an uncorrelated background event.[14]

These events, correlated or uncorrelated, are caused by three different sources: fast neutrons, natural radioactivity, and ^{8}He/^{9}Li decays. Fast neutrons are high-energy neutrons produced in muon-nucleon interactions. In the case of the Daya Bay experiment, the fast neutrons can be created outside the water pool by cosmic muons interacting with the surrounding rock. These fast neutrons can result in a recoiling proton followed by a thermal neutron capture. Upon capture of the thermal neutron, the detectors would view it as a delayed event from the prompt signal, which was given by the recoiling proton, and interpret the data as inverse beta decay. ^{8}He/^{9}Li are isotopes that are created by incoming muons, and they have a high percentage beta neutrino of decays that can emulate inverse beta decay, with the beta energy posing as a prompt signal, and the emitted neutron thermalizing and capturing.[14] The muon system is meant to detect the parent muon for these events, so that they may be subtracted, though it is also partially possible to reduce this background, lowering the number of events that need to be detected. It is possible to detect muons before they create the background, so

that they may be rejected from the system and any and all events they create are thus removed from the data system.[14]

If an event occurs involving the passage of a muon less than 200μs before the prompt signal, it can be removed from the collected data sample without too much deadtime. This passage is not guaranteed to create a fake signal event, in fact the probability is fairly low, but they must be accounted for regardless. Not all events that occur will be detected by our methods, and so we must find a way to extrapolate the undetected muon events. This involves measuring the energy spectrum of the events that are actually detected. We must also know the exact inefficiency in 'tagging' events, and use this knowledge to estimate and statistically subtract the unknown background with an uncertainty smaller than 0.1%.[14]

2.2 Noise Removal:

There are three different aspects to noise detection/removal, and all three add together to result in an accuracy level of the data that is above 99.5%.[14]

2.2.1 Overburden:

The first aspect of noise removal is the use of overburden. This consists of placing the detectors beneath the mountain, so that the soil above can act as a shield.

Each set of detectors (near and far) is set beneath the mountain, but the amount of overburden is different for each. Part of the reason is, of course, that the near detectors need to be close to the anti-neutrino source, i.e. the power plant. Given that the power plants are all above ground, next to mountainous terrain, the near detectors are beneath the mountain, but in order to catch the majority of antineutrinos emitted from the source, they are close to the plant, thus the overburden is low. Their positions are thus: the Daya Bay near detector is 363 m from the Daya Bay cores, and the Ling Ao near detector is 481 m away from Ling Ao cores, and 526 m from the Ling Ao II cores.[14] A less engineering driven and more detection driven reason for the position of the detectors at those distances is the need to improve the optimization of the oscillation maxima. Because the detectors are beneath a mountain, the overburden will increase the deeper into the mountain the halls are excavated, and thus the background will decrease as a

result, allowing it to be measured with greater certainty. But what is also important to note is that the further into the mountain the halls are, the further away they are from the source, thus less antineutrinos enter the detector. These two factors even out, resulting in a mostly constant background-to-signal ratio.[14] "The overburden requirements for the near and far sites are quite different because the signal rates differ by more than a factor of 10.'[14]

2.2.2 Resistive Plate Chambers:

While overburden is purely used to decrease noise level, the other two aspects of noise removal consists of measuring incoming muons, such that the data can be rejected in the antineutrino detectors. Resistive Plate Chambers, or RPCs, consist of two plates of Bakelite. The plates are kept parallel with the use of insulating polycarbonate spacers[16], with the area in between filled with a mixture of isobutane, Argon and Freon gas. This gas mixture was chosen because it requires a low operating voltage and because it is highly dense, and thus results in a high level of ionization.[16] With four layers stacked one above the other, and with each layer extending past the pool for 1m in every direction, the RPCs are designed for a 98.6% efficiency. The efficiency becomes 99.23% if one of the layers fails to work and the muon is only measured hitting 2 out of 3 RPCs. This increase in efficiency makes it seem as if using 3 layers of RPCs is better than 4 layers, but there is a disadvantage to such a setup. With three layers there is a higher chance of accidental triggering, that is, a higher chance that a muon will be detected when there is no muon present. This is acceptable on occasion when one of the four layers temporarily ceases to work, but results in too much dead time if done over the entire muon array.[14]

The RPCs work as follows: when a muon passes through, it ionizes the gas. A high voltage is applied across the gas gap whose purpose is to create a strong electric field in the gas of the RPC. This field caused the ions and electrons produced in the gas to move towards the Bakelite electrodes producing a current inside the RPC which is registered on segmented pickup strips sending an electrical signal to the data acquisition system.[14] Thus the RPC records the time and position of an incoming muon, and this information is used to remove associated activity in the antineutrino detector. Because

there's a chance that the particle is either not a muon, or is incoming at such an angle that it will not hit the pool, there is a requirement that three of the four layers of RPCs detect a hit in a certain amount of time. That is, within 20ns of the first RPC being hit, two others below it have to be hit as well, or it will be assumed that a muon did not pass through.[14]

2.2.3 Water Pool:

Beneath the RPCs is the water pool. The pool has a dual purpose. The antineutrino detectors are placed in the center of the pool, with 2.5m of water between them and the edge of the pool in each direction. The water pool's first purpose is to act as a buffer, to stop fast neutron and gamma rays produced outside the pool, thus reducing the amount of noise entering the antineutrino detector. The pool's second purpose is to cause passing muons to emit Cerenkov radiation, which PMTs set up around the pool would detect.

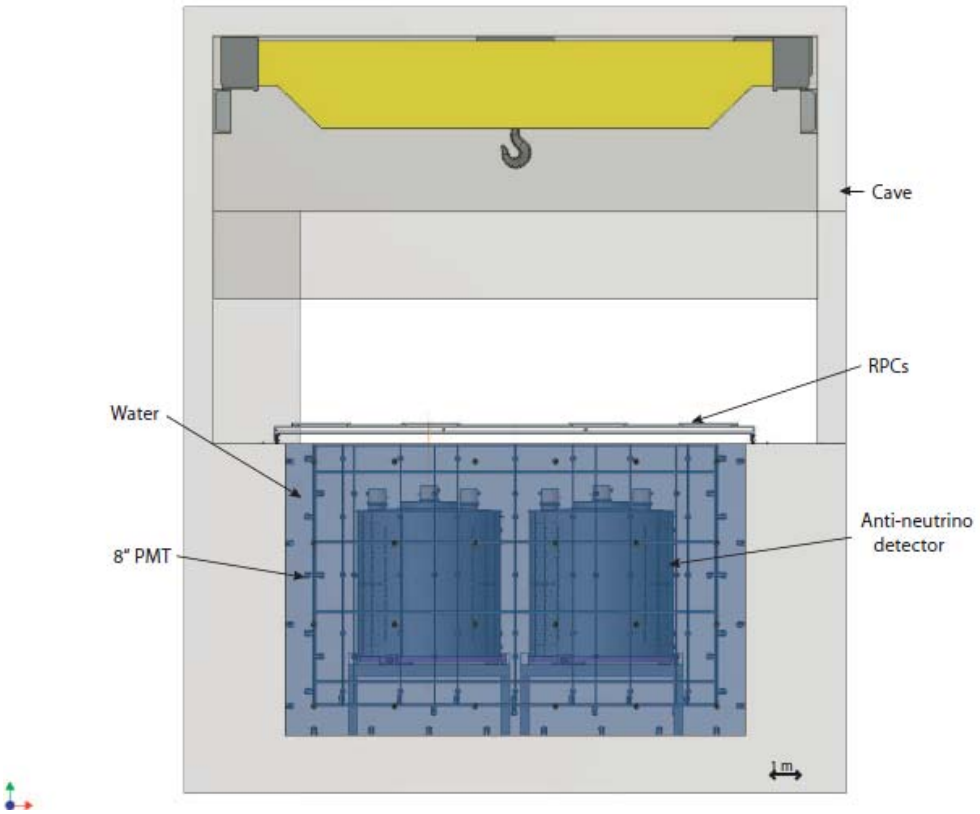

Fig. 2.1 Side view of detectors in muon pool[14].

For the Cerenkov counter to be effective, the coverage of the pool by PMTs needs to be carefully chosen. The pool dimensions are 16m sides (length and width), and the height is 10m. Along the edges of this pool are PMTs mounted facing inside, towards the detectors.

2.2.3.1 Setup of the Water Pool:

Now that I have outlined what we need to measure, we can see what the system looks like. The antineutrino detectors are in a large pool of water, with 1m separating them from each other, and a minimum of 2.5m separating them from the edge of the pool. The pool is octagonal; it looks like a square with the corners cut off at 45º. This is the case of the far hall. The near hall is smaller. It is in the shape of a rectangle with the corners cut off, with the sides being 16mx10m instead of a 16m square.

Around the edge of the pool there are PMTs lined up to detect the Cerenkov light emitted by impacting muons. They are positioned between the inner and outer section of the pool, in the 1m thick area surrounding the pool. They are supported by a stainless steel frame covered with Tyvek film 1070D reflectors. In addition, RPCs are placed above the pool, extending 1m beyond the edge on all sides of the pool.[14]

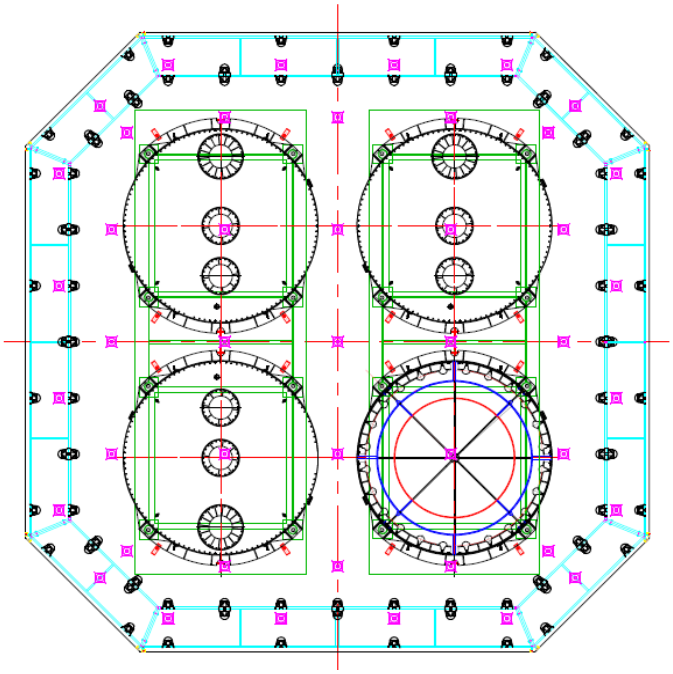

Fig. 2.2 Top view of muon pool, with detectors and PMTs visible[14]

The muon system consists of antineutrino detectors placed in a water pool. The pool is octagonal, and of size such that the shortest distance between the detector and the nearest wall is 2.5 m. This distance was chosen for the purpose of reducing the gamma flux created by the surrounding rocks. The 2.5m result in a decrease in gamma flux of about five orders of magnitude.[14]

The pool also has the purpose of attenuating the flux of neutrons that are produced outside of the water pool. In other words, it acts as a buffer for flux due to surrounding rock and neutrons created outside the pool.

In building three layers of muon blockage and detection, we are attempting to create an overall efficiency of detection that is 99.5%±.25% or higher. So we have redundant systems set up to achieve this number. We have two tagging systems set up for cross-checking, which are the RPCs and the Water Cerenkovs. As stated earlier, we also have a method of extrapolating the undetected background using the energy levels of tagged muons and the uncertainty of detection.[14]

The third layer is the water shield. Incoming muons interact with any available material, including the rock surrounding the water pool. This interaction can result in a fast neutron background, and the water shield is used to reduce this background. For every 50cm, that water reduces the background by a factor of 1.5-2. The water also causes the muons to emit Cerenkov radiation.[14]

2.2.3.2 Cerenkov Radiation

The use of the pool as a Cerenkov radiation detector is an important part of the experiment, and a quick summary of the physics of Cerenkov radiation is needed before the experiment itself is examined. The speed of light in water is not an impassable constant, it is equal to c/n, with c being the speed of light in vacuum and n being the index of refraction of water. Therefore, while it is not possible for massive particles to travel at the speed of light in vacuum, it is quite possible for them to surpass the speed of light in a given medium. And that is precisely what the muons in this experiment do when they enter the water pool.

Much like a sonic boom occurs when an object passes the speed of sound, a "light" boom occurs when a charged particle surpasses the speed of light in a given

medium. When the particle begins traveling faster than the speed of light, a cone of light, called Cerenkov radiation, is emitted at an angle equal to $\cos^{-1}(1/\beta n)$ with respect to the trajectory of the particle. To understand why this cone of light occurs, a quick look at the electromagnetic forces present is needed. A charged particle always interacts with a present electromagnetic field because it emits its own electromagnetic field. As the particle travels, its own emitted field interacts with the field present in the material it is traveling through. This interaction within a given medium consists of the particle's emitted field displacing and polarizing the atoms of the medium. Following the displacement, the particle and its EM field pass away, causing the displaced particles to realign themselves to their original positions. In the process of this realignment, they emit photons. This interaction and emission always occurs, regardless of particle speed, but a light cone is only emitted when the particle is traveling faster than c/n. The light cone does not occur for smaller velocities because the photons interfere destructively for all speeds below c/n, but they interfere constructively for higher speeds.[17]

From this analysis of Cerenkov radiation, it shows that every time a muon traveling faster than the Cerenkov threshold enters the pool, a conical flash of light is emitted. There are PMTs set up everywhere around the pool at an approximately equal distance from each other along the wall and along the bottom of the pool.[14] Their purpose is to measure these flashes of light. They are not part of the antineutrino detector; their only purpose is to detect muons that will interfere with the system. The PMTs are set up such that when a muon enters the pool and emits light, its presence and trajectory will be known. Therefore, if it's on a trajectory to hit the antineutrino detector we know to ignore data coming in at the given time during which that muon would be within the detector.

2.2.3.3 PMTs:

Following the scientific analysis of Cerenkov radiation, it is now important to review the physical aspects of a PMT in order to understand the way the detectors work. PMTs are "electron tube devices which convert light into a measurable electric current"[18]. There are several parts to a PMT; within a long tube, there is a progression of materials designed to increase the effect of an incoming photon, such that its

appearance is easily measured. The outward facing part is where the photon enters, it is a photosensitive cathode. The cathode is then followed by an electron collection system that opens into a section that consists of a string of dynodes, whose purpose is to multiply the incoming electrons. The dynode string leads into an anode, the part that collects the final signal to be recorded by our data acquisition system.

To run the PMT, a high voltage is applied such that the cathode is at ground and each dynode is at a successfully higher potential up to the anode, causing a potential "ladder" along the structure. When a photon enters the PMT and hits the cathode producing an electron through the photoelectric effect. The electron is then accelerated by the potential difference to the first dynode, where it transfers some energy to the electrons in the dynode. This transfer results in a second set of electrons being emitted and accelerated towards the next dynode. The same thing happens there. The continual transfers result in a geometrical increase of electrons traveling down the dynode chain "with a gain as high as 10^6 and with an effectively low noise level.'[19] At the end of the dynode chain, the anode waits to collect all the incoming electrons, which it then emits as a current that is recorded for computer for analysis.

The PMTs will read out the incoming photons in a linear manner. That is, for any number of photons entering the PMT, "the current at the output of the PM will be directly proportional to the number of incident photons.'[18]

Chapter 3: Calibration and Hardware

All aspects of the Daya Bay experiment need to be carefully weighed before they are put into operation. To that end, each part of the experiment that involves data taking needs to be calibrated before being put into operation. The experiment involves collecting data from the antineutrino detectors through the use of PMTs, whose efficiency needs to be measured. Therefore the PMTs in the antineutrino detector need to be calibrated. Outside of that, there are PMTs being used to measure the influence of outside sources. The muon detection system uses PMTs lined around the tank facing the anti-neutrino detectors. These PMTs need to be calibrated as well. The work being done at Virginia Tech involves the calibration of the PMTs used in the muon detection system.

3.1 Work at Virginia Tech:

3.1.1 Simulation:

The work consists of two parts. Jonathan Link, Daniel Baker and Debabatra Mohapatra worked on a program simulating the behavior of the PMTs and LEDs in the muon system, in order to measure the correct position for each PMT. The program involved aligning the PMTs and LEDs such that one several PMTs receive hits from one LED. With this reasoning, all PMTs should be hit by the least number of LEDs possible. The light source simulated is an LED in a diffuser bulb, so that the light emitted is isotropic. The radial distance of the PMTs from the LED is between 1m and 5m. The electronic simulation is used to measure the number of photoelectrons emitted by the LED.[20]

3.1.2 Pulsar Card:

Aside from the simulation, we are also working on the hardware aspect of this experiment. Namely, the pulsar card used to pulse the LED and the study of the diffuser ball used to make the LED isotropic. We first attempted work with a relatively large pulsar card that was meant to send 4ns wide pulses to the LED. We discovered a problem with this idea, however, in the form of noise. The card emits a pulse of noise that is picked up in the PMTs every time it pulses the LED. For low-light LEDs, the noise detected from the card was higher than the pulse detected from the LED. The noise

level was lower when the LED was connected directly to the pulsar card, and it lowered significantly if the high voltage used to power the card was lowered from its high of 195V. We ran it at 50V, and the noise level was highly decreased. Of course, the number of emitted photons was also much lower. The other issue was that the LED would not be directly connected to the pulsar card in the experiment while it runs. This is an issue because the noise did not stay contained to the pulsar card. It was detected from the card itself and from the wire connecting the card to the LED. The wire acted like an antenna. We attempted to create a Faraday cage to stop the signal, but our attempts failed. We at first attempted to use tinfoil, and followed that with an attempt to use a copper wire. Neither showed much success. We used lemo cables and BNC cables to see what the difference would be. The noise level seemed to exist throughout the cables, though it spiked at the metal junctions that connected one cable to another. Therefore connecting the LED to a pulsar card with any sort of cable will result in that cable acting as an antenna and emitting the noise signal.

3.1.2.1 Measuring the Noise:

Our first attempt to take data from the diffuser ball showed us the noise from the card. With the high voltage across the PMT set to 1600V, we connected a diffuser ball to the pulsing card and placed it in the dark box, separated from the PMT by a wooden plank, to avoid flooding the PMT with too much light. The resulting graph on the oscilloscope had several short peaks before the LED pulse. To check whether these peaks were due to the diffuser ball, we switched it out with a simple blue LED. The image on the oscilloscope had the same short peaks, but the LED pulse was lower. The pulse was lower because the LED was not facing the direction of the PMT, therefore most of the photons were not detected by the PMT. The same was not true for the diffuser ball, as the light emitted through a diffuser ball is equally distributed in all directions.

Proving that the noise was not due to the diffuser ball, we attempted to determine whether the noise was a constant source of light entering the dark box from elsewhere. We turned off the LED and ran the PMT. We saw no hits, thus our box was well-insulated, and the noise was coming from within. To test this theory, we turned the PMT

voltage down to zero, but kept the LED lit. The PMT should not have been able to detect any light. And in fact, there was no pulse shape due to the LED visible on the oscilloscope, but the short peaks were still visible. Our conclusion was that the peaks were cause by electromagnetic interference from the pulsing card.

In addition, we tried several attempts to figure out where exactly the noise comes from. We created an antenna by attaching a lemo wire to the oscilloscope and letting it hand free so that it could pick up noise from the environment. Then we played with the power supplies sent to the pulsar card. First we kept everything plugged in, then turned off the 195V and/or 15V power supplies; in both cases the noise disappeared. If we kept those on and unplugged the 5V trigger, the noise disappeared. If we changed the trigger from 5V to 3V, the noise was still there. If we altered the shape of the TTL and made it less of a square wave, the noise was still there. We increased the rise time up to 1μs on the TTL, and saw no change. If we increased the rise time to 2μs, the noise disappeared. However, we believe that this was not due to the pulse shape, but was in fact due to time being too high to drive the card, as the LED was no longer flashing.

In a different attempt to lower the slope of the TTL we used a low-pass filter to smooth out the edges; we used a 20 ohm resistor and a 1nF capacitor between Vin and Vout. It worked; The peak of the TTL was still at 3V, the LED turned on, but the signal built slower and the noise was lowered. The noise level was halved; the highest level was at 10 mV, compared to the 20 mV without the filter.

We attempted to calculate the error systematically by moving the chip close to and away from the lemo cable in the oscilloscope. If we only used a short lemo cable as our antenna, the noise level was close to 0V, so it was not a very effective antenna. We changed it to a longer lemo cable, and the noise level reached 10mV in amplitude. With this antenna, we moved the chip away from it in 10cm increments. We did three data runs and took the average. We graphed the data in x vs. 1/y form, and the result was a linear relationship. Therefore, the pulsar acts like a radiating dipole, where the power drops off as 1/r.

Therefore our solutions to reduce the noise level emanating from the card involve the following; don't use a long antenna to connect the card to the pulsar, lower the high voltage sent to the pulsar from the current 195V, decrease the slope of the TTL, and wrap

a ground braid around the PMT. Unfortunately, except for the ground braid wrapped around the PMT, all of our solutions are not feasible in the experiment.

We have since then decided to use a different pulsar card to power the LED, a small one that will go inside the diffuser ball, therefore the problem of the antenna will be solved in this manner. The noise level and efficiency of this pulsar card is being tested by Debabatra Mohapat, postdoc at Virginia Tech working on the Daya Bay project.

3.1.3 Diffuser Ball:

In addition to work with the pulsar card, we have been working on the type of diffuser ball that will be used in conjunction with the LED. The first prototype was a type of diffuser ball created in China exclusively for this project. The ball was discarded, however, because there were too many air bubbles inside the plastic, resulting in emitted light that was not uniform enough for our purposes. We have since then settled on using Teflon balls. Upon first look, they seem too opaque to allow any light through from the LED, but upon testing we saw plenty of light being emitted. Our only issue now is to ensure that the acrylic used to hold the LED within the ball can stick to the Teflon surface.

3.2 LEDs:

My work on this experiment involved the study of the LEDs that will be used within the diffuser ball. I measured the spectrum of several LEDs, both the kind that are meant for use in the experiment, and others of different colors purely for comparison's sake. I also recorded the detection of photons over a certain period of time, in an attempt to determine whether the LEDs emitted light in the form of fluorescence after the initial burst of light coming from the pulse.

The experimental setup for the study of LEDs involved the use of a high voltage power supply for the PMT, three power supplies for the LED, a discriminator, a coincidence unit and an ADC for data collection.

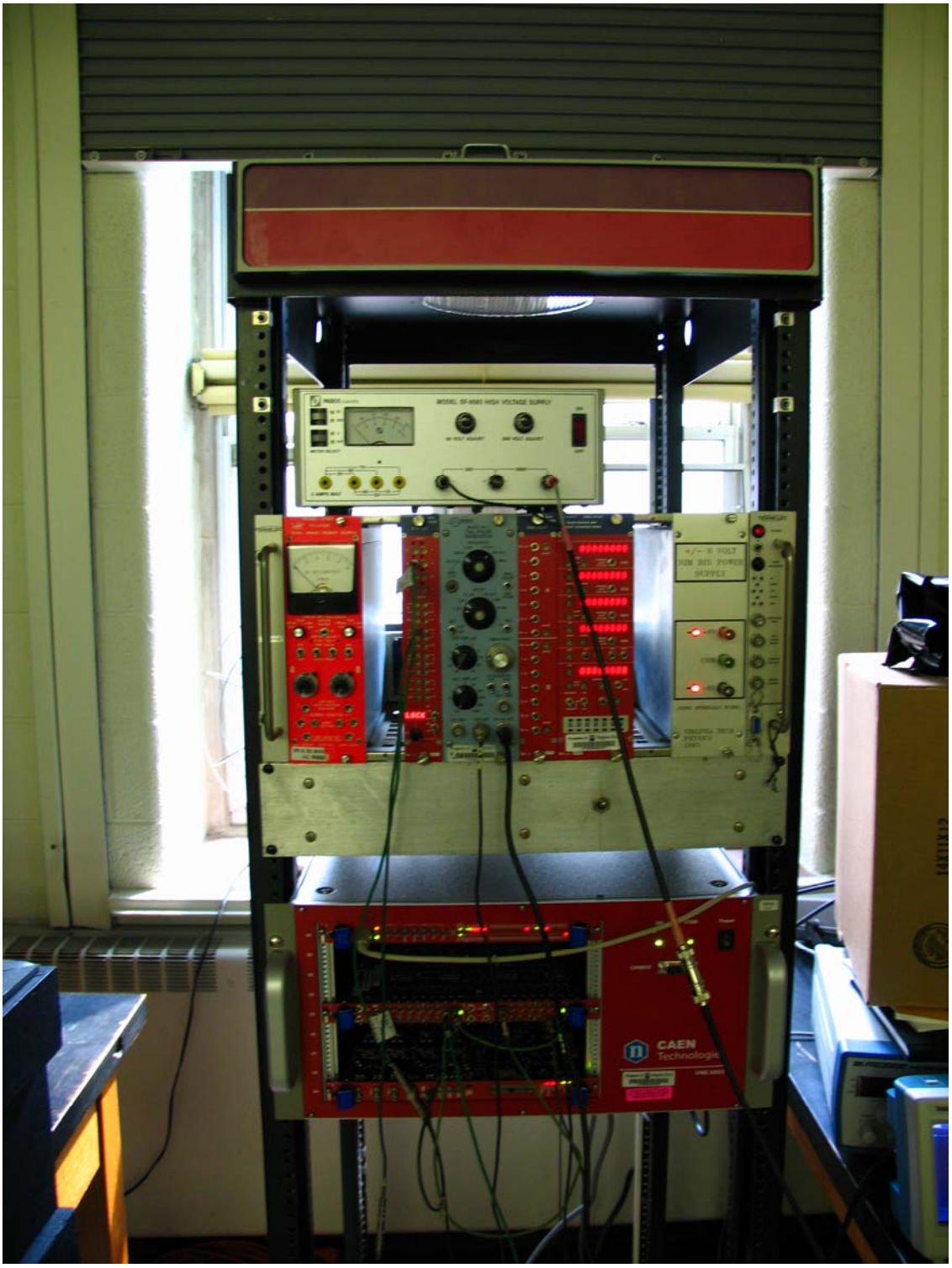

Fig.3.1: DAQ setup: PMT into ADC and discriminator, from discriminator to coincidence unit, trigger into pulsar card and coincidence unit, coincidence unit set to AND into ext. trigger of ADC.

The high voltage for the PMT was set at 1850V, our upper limit for detecting data while keeping the noise from overwhelming the results. The PMT was placed inside a dark box, thus keeping all ambient light from entering the LED and interfering with the light from the LEDs. The LED was connected to the PCO 7710 pulsing card from DEI. The card needs three sources of power input in order to work; a 5V TTL trigger, a 15V support power input, and a 195V high voltage power input which determines the pulse voltage of the card.[21]

Chapter 4: Data and Analysis:

4.1 Choice of LEDs:

There is a great deal of care put into the decision of which LED will be used for calibrating the muon pool PMTs, and my work provides only part of the information needed to decide on the best choice. There are several parts to the equation. First, our water pool is meant to detect Cerenkov light, therefore our LEDs should imitate the wavelength of Cerenkov light to be useful. The plot below shows that Cerenkov light is more abundant at lower frequencies. That's one factor to consider.

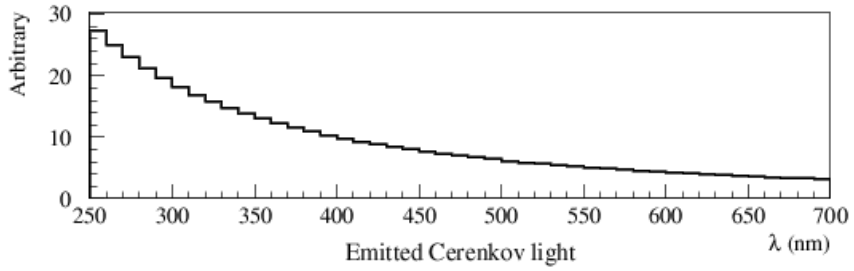

Fig. 4.1 Measure of Cerenkov light detected by PMT by wavelength[22]

A second factor we need to deal with is the attenuation of the water. The plot below shows how water attenuation depends on wavelength of light. The highest rate of photons is transmitted through the water in the 300nm to 500nm range.

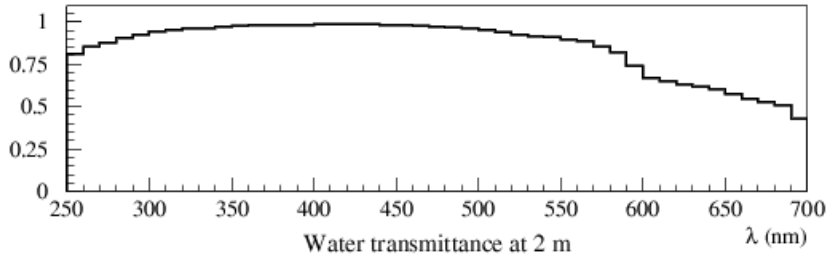

Fig. 4.2 Measure of light detected by PMT separated by 2m of water, dependent on wavelength[22]

The third factor we must take into account when choosing LEDs is the quantum efficiency (QE) of the PMTs. PMTs will only detect light within a certain wavelength, and will be more effective at some wavelengths more than others. The plot below shows the QE of a PMT peaks slightly before 400nm, so that would be the ideal wavelength in terms of detection efficiency.

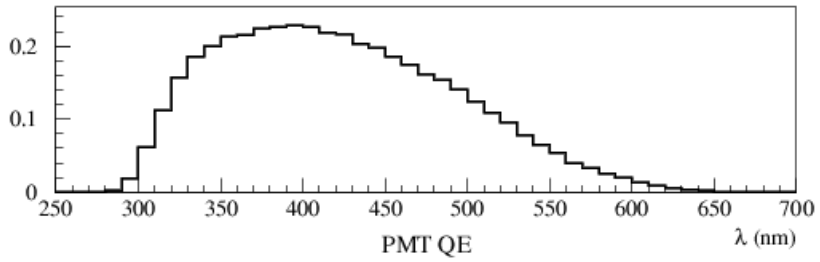

Fig. 4.3 Measure of quantum efficiency (% detected) as a function of wavelength[22]

Combining these three plots, we find that the ideal LED lies between the 365nm and 430nm wavelength range. This plot led us to focus our study on UV LEDs as well as a blue LED with a 430nm spectrum.

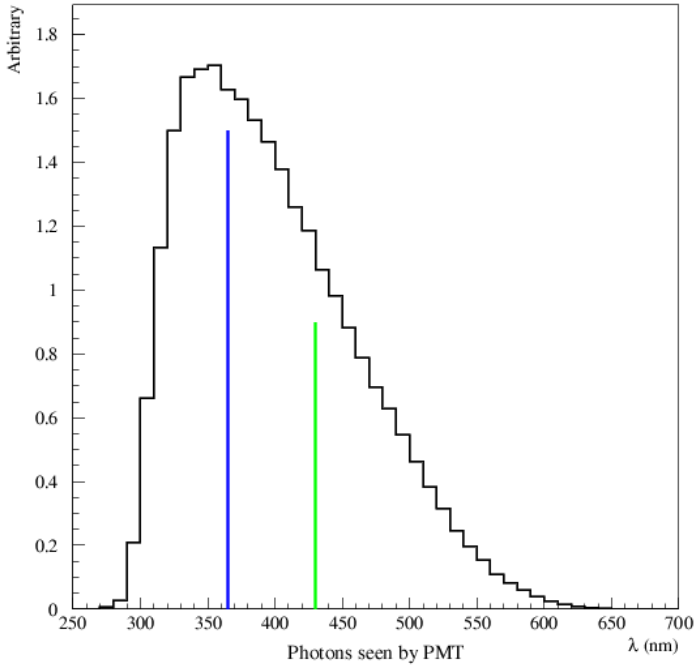

Fig. 4.4 Photons detected by PMT as a function of wavelength with the attenuation, QE and Cerenkov spectrum taken into account.[22]

4.2 Spectra:

For our first run of data, we simply measured the spectra of some blue LEDs that were meant to be used for the experiment. The blue LEDs chosen were designed to have a peak at 430nm. We ran the test on two different kinds; the IHEP LEDs sent to us from China that were meant to be used in the experiment, and another set of commercial LEDs

that had the same wavelength. The resulting spectrum was identical for both. Depending on how wide the aperture on the spectrometer was, the peak varied in magnitude, but not in position. Also of note; all LEDs have a certain amount of angular dependence. The light is only emitted up to a certain angle from the top of the LED. Because of this dependence, I faced all LEDs straight into the PMT, in order to increase the rate of photons detected.

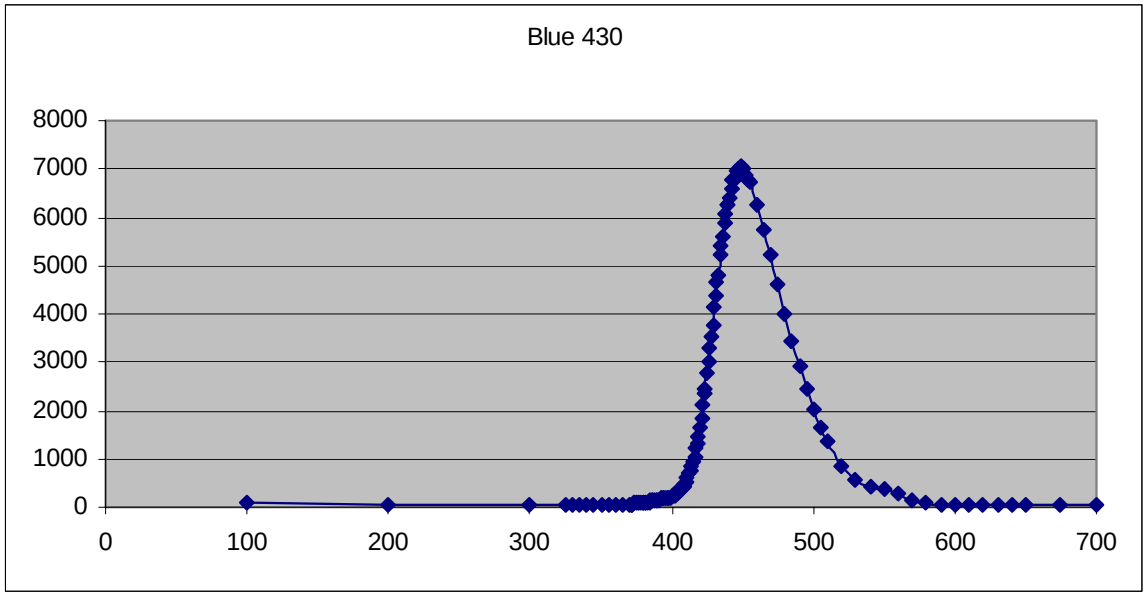

Fig. 4.5. IHEP LED. PMT Voltage (mV) vs. Wavelength (nm). Spectrum of LED with 430nm peak.

There were, in truth, two peaks, one at 388nm and one at 440nm, but when we allowed more light in the peak at 440 grew in amplitude, while the one at 388nm did not, and thus is barely visible in the above graph. The graph below, measuring the same LED will less light input, shows the second peak quite clearly.

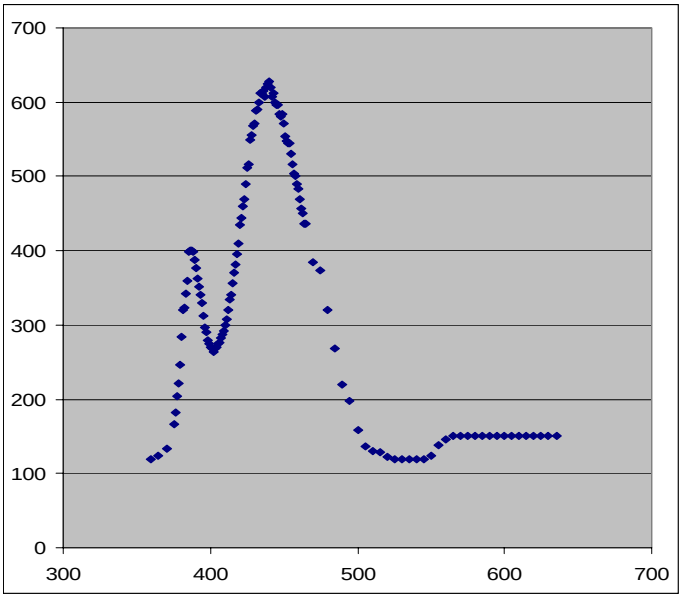

Fig. 4.6. IHEP LED. Voltage (mV) vs. Wavelength (nm). Spectrum of 430nm LED at lower voltage input.

For comparison's sake, we then measured the spectrum of a commercial blue LED with a 470nm peak. The end result is one peak at 470nm, with a slightly narrower range of wavelengths of 100nm, in comparison to the approximately 150nm range of the 430 blue LED.

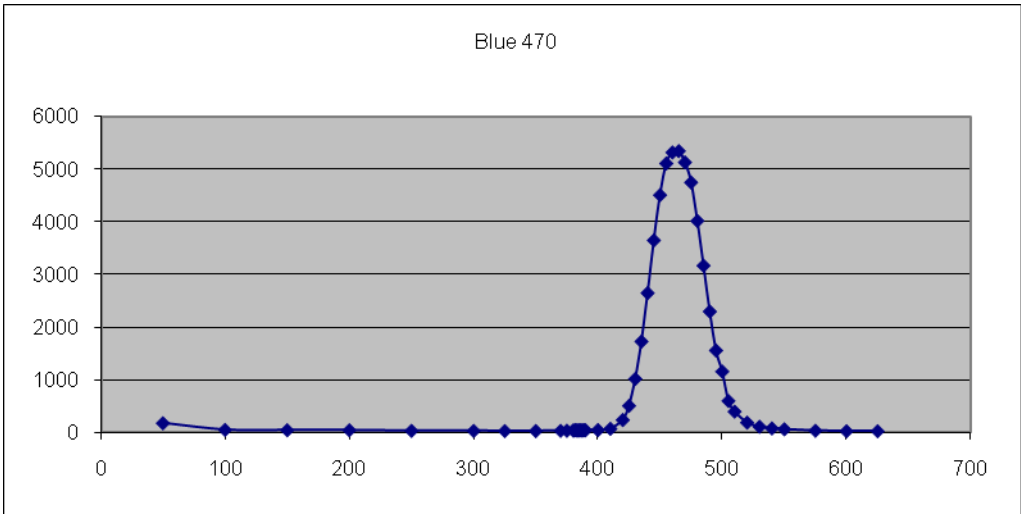

Fig. 4.7 Chicago Miniature LED. Voltage (mV) vs. Wavelength (nm) Bright Blue 470nm LED spectrum

Following the spectra of the blue LEDs, we measured the spectra of two UV LEDs, in case we chose to use them for the calibration of PMTs instead. We used

commercial LEDs from the NICHIA corporation. The 375 UV LED had two peaks at 315nm and at 375nm, instead of just one peak at 375nm. The height of the peaks varied on the day, though the position was constant. I believe this LED is even more sensitive to angle of incidence than the previous ones, and the relative peaks depend on the angle the LED is positioned towards the PMT.

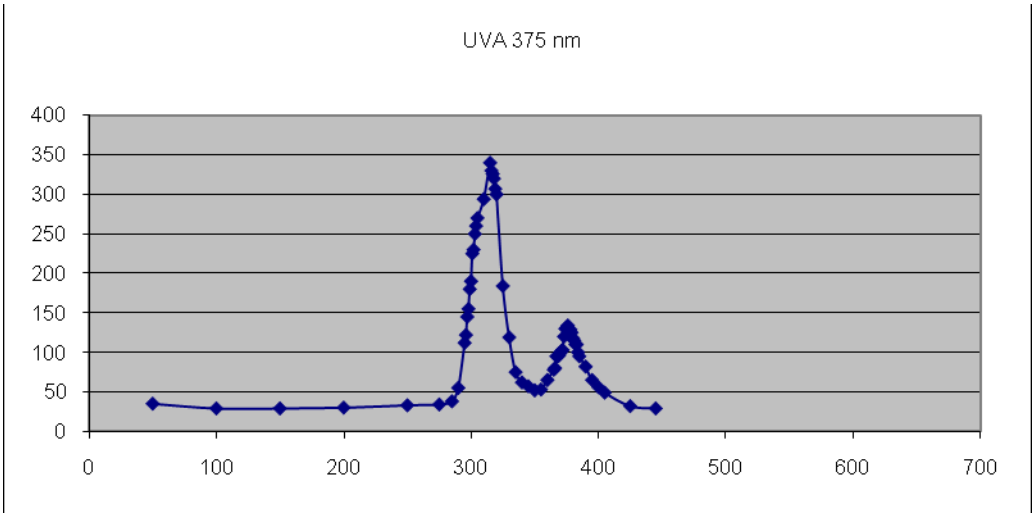

Fig. 4.8 NICHIA LED[23]. Voltage (mV) vs. Wavelength (nm) UV 375nm spectrum.

The 365 UV LED does not have this issue. It has one spike at 365nm, with a width of ~70nm, the thinnest thus far.

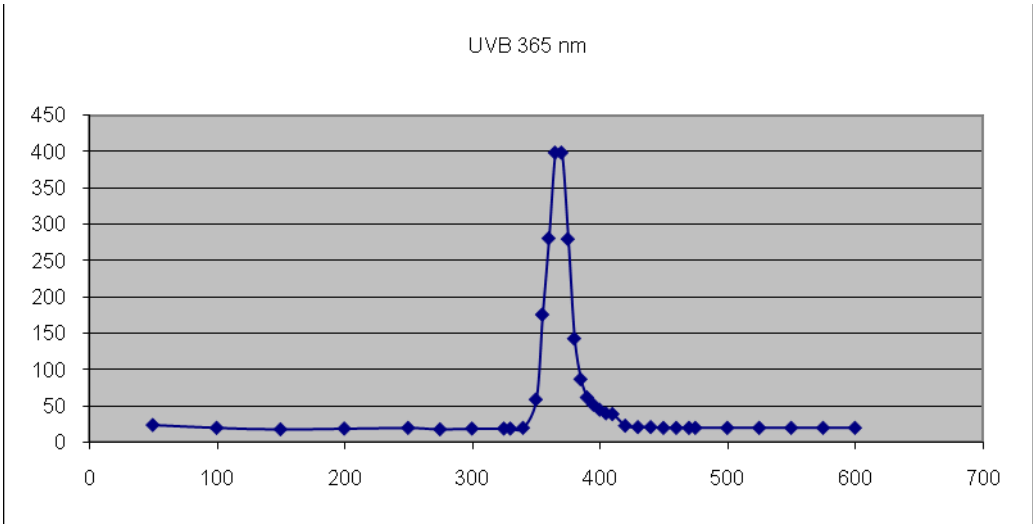

Fig. 4.9 NICHIA LED[24]. Voltage (mV) vs. Wavelength (nm). UV 365nm spectrum.

To compare, all the LEDs had peaks at the expected wavelengths, even if they had more than one. In addition, the UV LEDs had thinner spectra than the blue LEDs. The blue 430 LED had two combined peaks, and spectral width of ~150nm. The blue 470 had one peak and a spectral width of ~100nm. The 375 UV LED had two separate peaks of ~50nm each, and the 365 UV LED had one peak of ~70nm width.

We attempted to precisely determine why the spectrum was so wide for these. We suspected that the LEDs were emitting fluorescence due to the plastic material of their lens, and that was what the PMT was picking up towards the longer wavelength end of the spectrum.

We decided to test two more LEDs of different colors for comparison's sake. We used a red LED with clear 'plastic' that had two peaks; one at 645nm, and one at the orange end of the spectrum at 565nm. The width of the peaks was 50nm and 90nm.

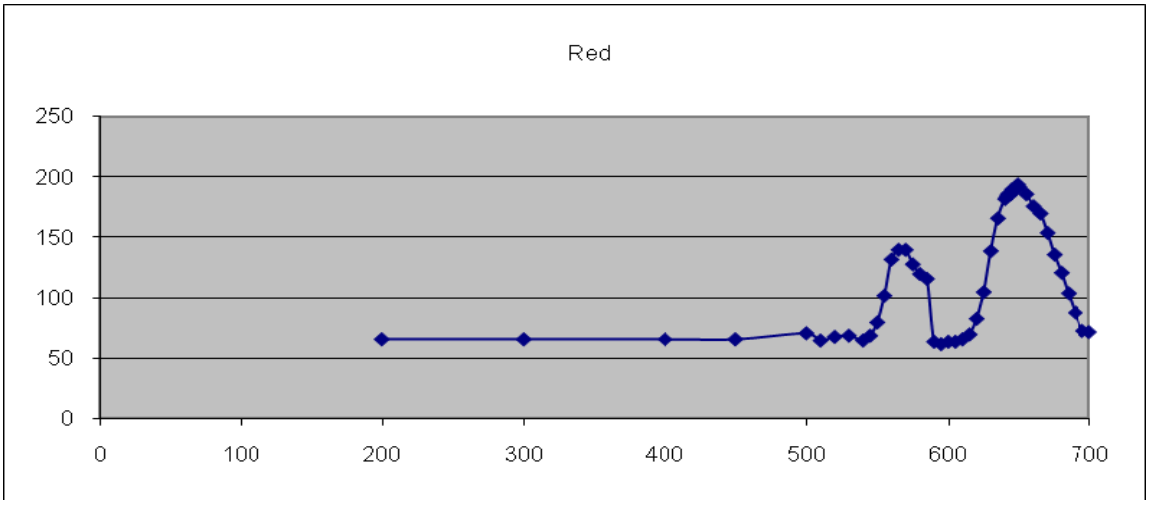

Fig. 4.10 Red LED spectrum. Voltage (mV) vs. Wavelength (nm)

We also used a green LED that was made with green 'plastic.' It had a peak at 560nm and a spectrum width of 100nm.

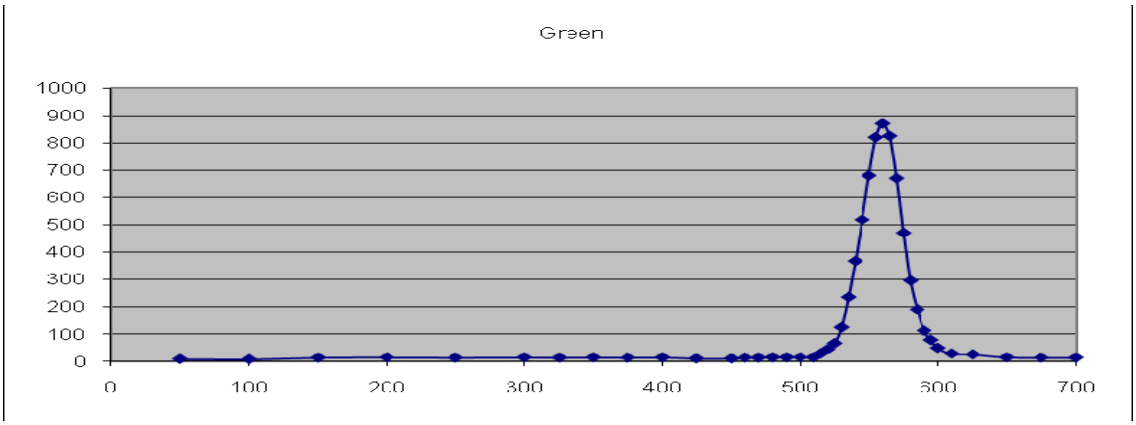

Fig. 4.11. Green LED spectrum. Voltage (mV) vs. Wavelength (nm)

4.3 Fluorescence Analysis:

With these spectra, we moved on to determine if it was possible to see fluorescence by looking at each data run separately. To collect data, and to avoid collecting random bits of data that would come from the occasional stray photon, we used a coincidence unit and a discriminator. First, we had the output from the PMT connected to channel 1 of the ADC with a cable splitter. The splitter allowed the data from the PMT to be sent directly to the ADC, but it also allowed us to send the same data to a discriminator. We used the discriminator to set a threshold, so that only data above a certain voltage would be accepted as useful (we set the threshold to be 10mV). We connected a cable from the output of the discriminator to one input of the coincidence unit. We set the BNC pulse to be released at the same time as the trigger to the pulsar card, and connected the pulse to another input in the coincidence unit. We set the coincidence unit to the AND setting, turned the output signal to a NIM pulse, and connected it to the external trigger input on the ADC. This forced the ADC to only collect data when the pulse from the PMT and the trigger pulse occurred at the same time, thus minimizing the risk of data collected for random photons. The diagrams below illustrate the setup:

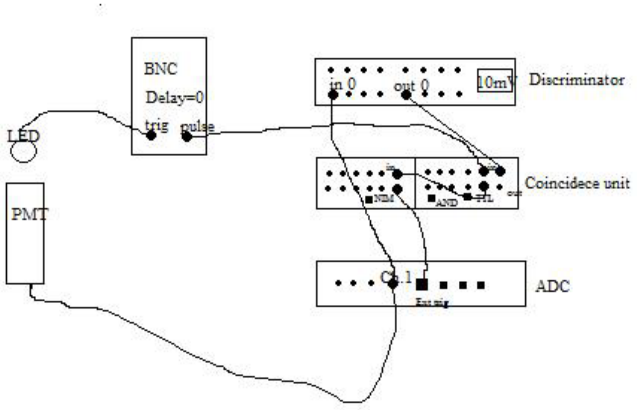

Fig. 4.12 Diagram of data acquisition system setup

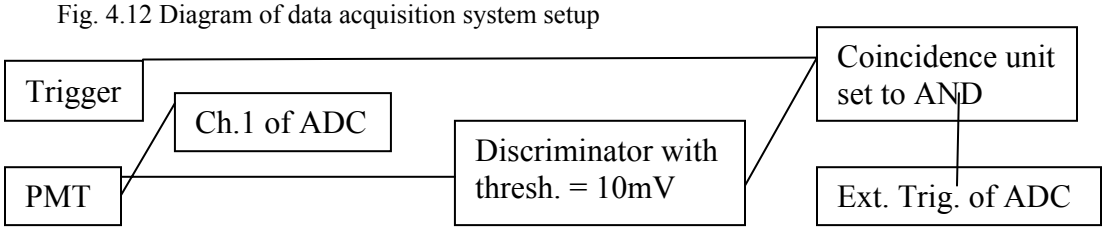

Fig. 4.13 Logic diagram of setup

We collected our data through the CAEN ADC, which we ran with an executable file created by a French school and sent to us by a CAEN representative. The program was created to resemble an oscilloscope. It contains all the options available to an oscilloscope, in addition to saving all of the data runs, for however long we chose to run the program. Each data run contained the voltage inputs during 2μs surrounding a pulse of light. The only limitation upon the digital oscilloscope in this program, which in fact came from the physical limitation upon the ADC, was that the voltage peak could not be larger than 500mV.

We ran our experiment by inputting a spectrometer in front of a PMT, choosing a wavelength, turning on the LED, and collecting data. The data we collected was the pulse shape from the LED out to 2μs past the initial spike, which ranged from 25ns to 525ns, depending on LED. We measured it at varying wavelengths, including at the spectral peaks for various LEDs. We were attempting to see if there was fluorescence coming from the LED. Fluorescence is the effect of light emitted from a material after being absorbed by it. The fluorescence in the LEDs would occur if the plastic of the LEDs retained some photons for a short period of time before emitting them again. It

could present itself as light detected at a wavelength that should not emit light for a certain LED, or it could be seen as light detected past the initial pulse. After we collected the data using the program (MATAQ.EXE), we cleaned it up and ran it through several programs in order to end up with a histogram with 5ns bins.

We created a program called Makefile.C mostly for the purpose of making the data look cleaner. Because the oscilloscope program was written by a French school, it uses the European method of separating and describing numbers. That is, thousands are separated by periods instead of commas, and columns are separated by semicolons instead of tabs. Therefore we wrote a program in windows and ran our data straight from the oscilloscope through it. This program also turned the raw data from the oscilloscope and turned it into a text file, so that the data could be accessed by any program we saw fit. Before running it through makefile.C, the data was in .cor form, which is simply raw data, but with a correction used to account for the calibration of the ADC.

Following Makefile.C, we ran the program through Chopped.C to remove unwanted data. The oscilloscope records data for four channels regardless of how many channels are connected. Since we only had channel one connected to the PMT in order to collect data, channels two through four collected only junk data. Therefore we ran the data stream through the chopped.C file to remove the three columns of useless data.

It is only then that we ran the program through Fluorescence.C. The Fluorescence program was written with the purpose of inputting the data from the ADC and turning it into a histogram. The file took 1000 runs of data and combined them into one text file that contained the information needed to create a histogram with 40 5ns bins.

Our results are enumerated below. The different lines are different wavelengths where the data was taken. The larger the line, the closer to the peak of the spectrum the data was taken.

Blue 430

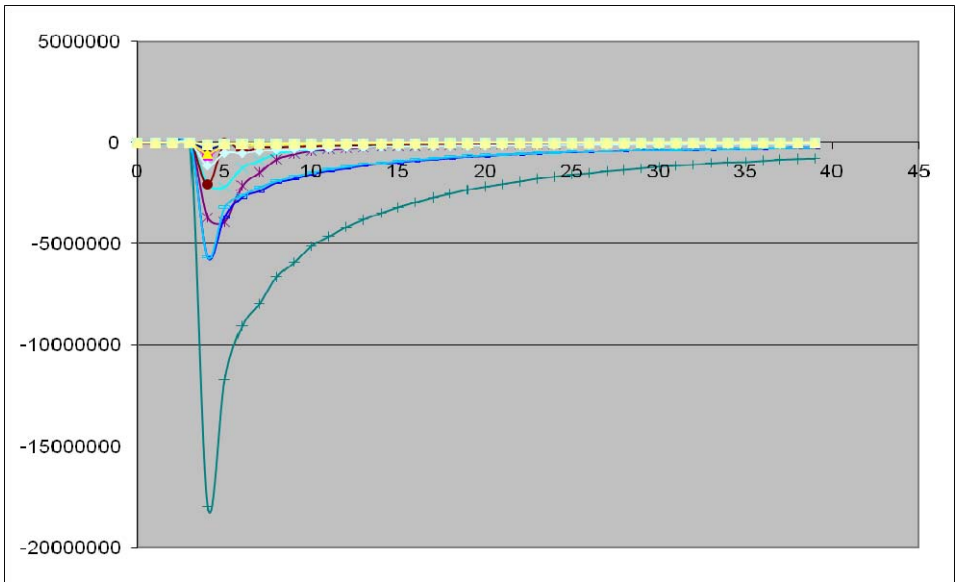

Fig. 4.14 PMT Voltage vs. Time for the Blue 430nm LED. Arbitrary units. The initial peak is the pulse and the slower decay is due to photons emitted later.

Blue 470

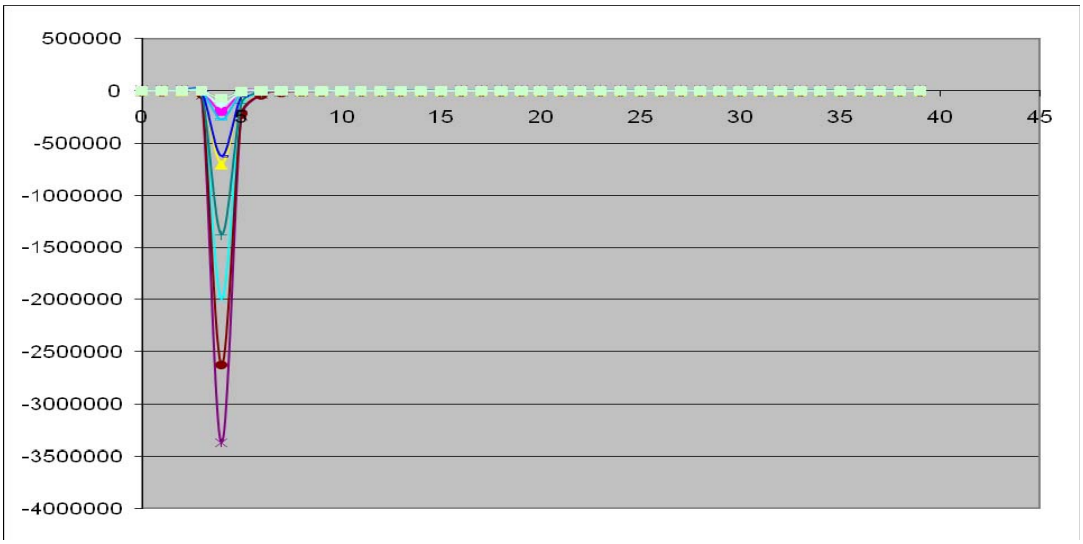

Fig. 4.15. PMT Voltage vs. Time for the Bright Blue 470nm LED. Arbitrary units. There is only an initial peak, so all photons are detected within the first burst of release.

UV 365

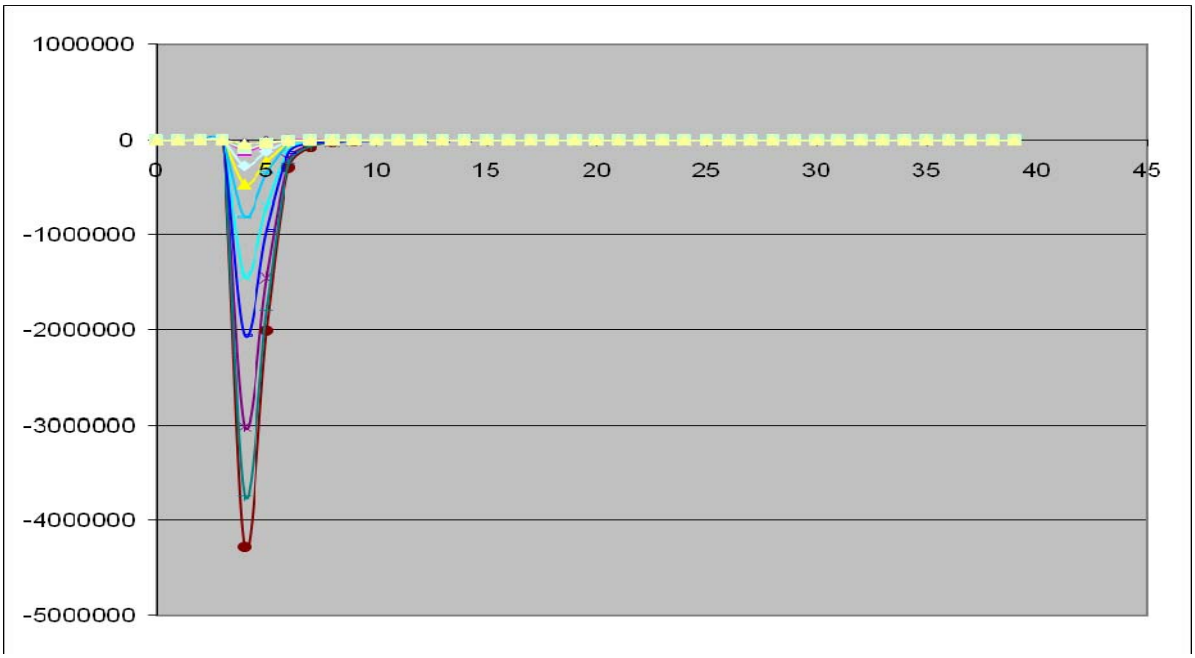

Fig. 4.16. PMT Voltage vs. time for the UV 365nm led. Aribtrary units. Most data collected in first burst, but there is possible delay for some photons.

Red

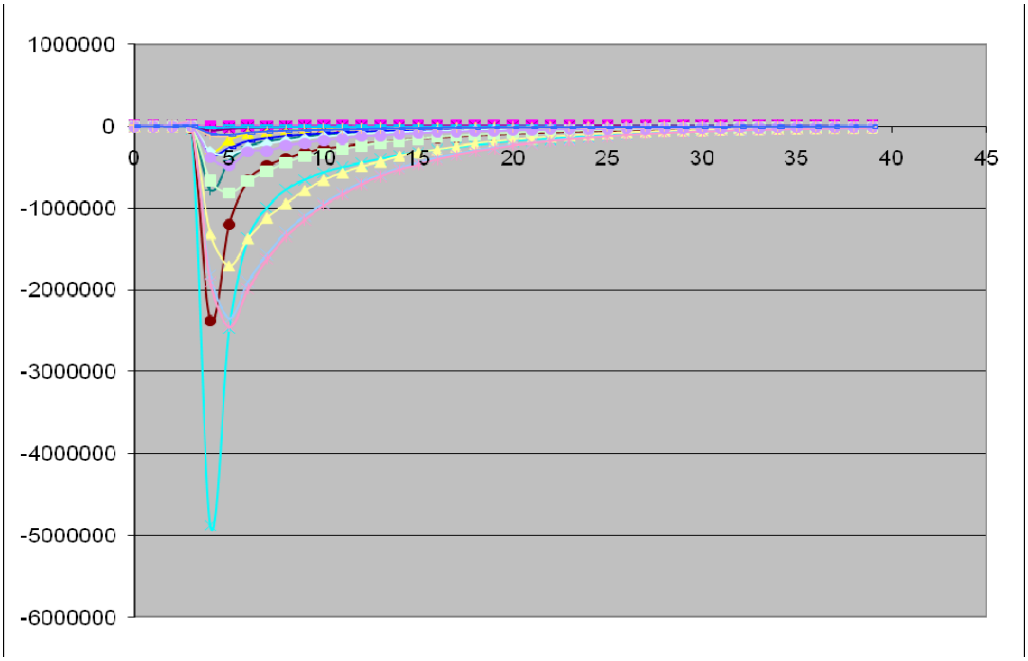

Fig. 4.17. PMT Voltage vs. time for the red LED. Arbitrary units. There is an initial burst followed by slower photons.

Green

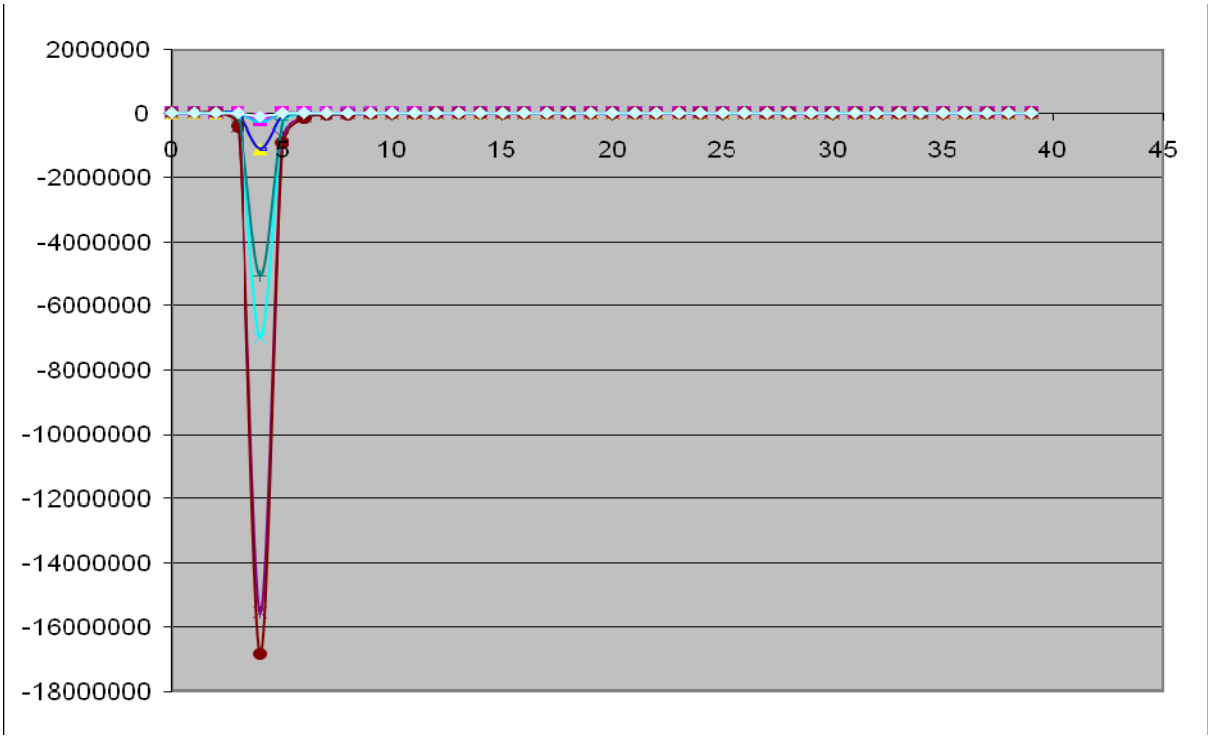

Fig. 4.18**.** PMT Voltage vs. time for green LED. Arbitrary units. All photons detected in initial burst.

Chapter 5: Conclusion

From these graphs we can see that in some cases, when the LED pulsed all the light was emitted and detected in that first pulse, while in other cases there was much more light being emitted after the initial pulse of light. The Blue 430 LED had a wide spectral peak, and its pulse in time is the widest in terms of emitted light. The next LED with the widest wavelength spectrum was the red one, and its pulse in time is not quite as wide as the blue 430, but it is wider than the rest. The next LED with the widest wavelength spectrum was the blue 470, which was on the same scale as the green, but they had they thinnest pulses in time visible. The 375 UV LED had two spectral peaks with a wavelength width of ~50nm, and its pulse in time is slightly wider than the blue 470 and the green. If the two spectral peaks were one, it would be the same width as the green and the blue, so the increased width of its pulse in time could possibly be affected by another factor.

All three spectral peaks that had a higher wavelength width to them; the blue 430, the red and the UV 365 had a longer pulse shape when observed in a time frame. This seems to imply that an LED with a wide spectrum is likely to have long tail end when the pulse is measured against time. This seems to suggest that the LEDs with wider spectral width do indeed produce fluorescence, as light is being emitted by the LED past the initial burst of the pulse. In future works, a comparison should be done between different LEDs with one spectral peak and their pulse widths, and LEDs with two spectral peaks and their pulse widths. In addition to this, a more in-depth study should be done of whether a wider spectrum width comes in tandem with a wider pulse width, and whether one is a cause of the other, or if they are both effects of another property of the LED.

Appendices:

Appendix A: makefile1.C

Makefile1.C

```
#include <iostream>
#include <fstream>
#include <string>
#include <sstream>

using namespace std;

int main() {
    string filestring;
      for(int k=0; k<=1000; ++k){
      stringstream myfile;
      myfile << "BlueXXX_" << k << ".cor";
      ifstream file1(myfile.str().c_str());
      stringstream ofile;
      ofile << "BlueXXX_" << k << ".txt";
      ofstream outfiletemp(ofile.str().c_str());
      cout << k << endl;
if (file1.is_open()){
      for(int i=0; i<2560; i++){
      file1 >> filestring;
      unsigned int r = filestring.find(",");
      while (r < string::npos){
            filestring.replace(r,1,".");
            r=filestring.find(",",r+1);
            }
      unsigned int p = filestring.find(";");
      while (p < string::npos){
            filestring.replace(p,1,"     ");
            p=filestring.find(";",p+1);
            }
      filestring.erase(18);
      //cout << filestring<<endl;

      outfiletemp << filestring <<endl;

      }
}
else cout << "Couldn't open file"<<endl;
      }
return 0;
}
```

Appendix B: chopped.C

```
#include "Riostream.h"
using namespace std;


void chopped(){
      float x, y,
w[40]={0,0,0,0,0,0,0,0,0,0,0,0,0,0,0,0,0,0,0,0,0,0,0,0,0,0,0,0,0,0,0,0,
0,0,0,0,0,0,0,0,0,0};
      ofstream myfile2 ("histdata.txt");
      for (int k=0; k<=1000; k++){
            int r=0, i=1;
            stringstream myfile;
            myfile << "/home/pediejo/Data1/out/BlueXXX_" << k <<
".txt";
            ifstream inFile(myfile.str().c_str());
            cout << k << " " <<endl <<"for loop repeat" <<endl;

            if (inFile.is_open()){

      float
s[40]={0,0,0,0,0,0,0,0,0,0,0,0,0,0,0,0,0,0,0,0,0,0,0,0,0,0,0,0,0,0,0,0,
0,0,0,0,0,0,0,0,0,0};
      int j=0;

            while (j<=39){
                  cout << "j while loop" <<j <<endl;
                  float z=0;
                  while(i<=50*(j+1)){
                        cout << "i while loop repeat" << endl;
                        inFile >> x >> y;
                        z=z+y;
                        cout <<"yo" <<i <<" "<< x <<" " << y <<endl;
                        i=i+1;
                        }
                  s[j]=z;
                  //cout << j <<" "<< s[j] <<endl;
                  j=j+1;
            }

      while(r<=39){
      w[r]=w[r]+s[r];
      cout <<"ha" <<r <<" "<< w[r] <<endl;
      r=++r;
      }
            inFile.close();
            }
            else cout << "Couldn't open file BlueXXX"<<k<<".txt"<<endl;
      }
      for(int l=0; l<=39; l++){
      myfile2 << l <<"  " << w[l]<< endl;
      }
      myfile2.close();
      return 0;
}
```

Appendix C: Fluorescence.C

```
#include <iostream>
#include <fstream>
#include <string>
#include <sstream>
using namespace std;


int main(int argc, char** argv) {
      int x, y,
w[40]={0,0,0,0,0,0,0,0,0,0,0,0,0,0,0,0,0,0,0,0,0,0,0,0,0,0,0,0,0,0,0,0,
0,0,0,0,0,0,0,0,0,0};
      ofstream myfile2 ("histdata.txt");
      for (int k=0; k<=1000; k++){
            int r=0, i=1;
            stringstream myfile;
            myfile << "/home/pediejo/Data/out/FluoXXX_" << k << ".cor";
            ifstream inFile(myfile.str().c_str());
            cout << k << " " << endl;

            if (inFile.is_open()){

      int
s[40]={0,0,0,0,0,0,0,0,0,0,0,0,0,0,0,0,0,0,0,0,0,0,0,0,0,0,0,0,0,0,0,0,
0,0,0,0,0,0,0,0,0,0};
      int j=0;

            while (j<=39){
                  int z=0;
                  while(i<=50*(j+1)){
                        inFile >> x >> y;
                        z=z+y;
                        i=i++;}
                  s[j]=z;
                  cout << j <<" "<< s[j] <<endl;
                  j=j++;
            }

      while(r<=39){
      w[r]=w[r]+s[r];
      cout << r <<" "<< w[r] <<endl;
      r=r++;
      }
            inFile.close();
            }
            else cout << "Couldn't open file
FluoXXX_"<<k<<".cor"<<endl;
      }
      for(int l=0; l<=39; l++){
      myfile2 << l <<"  " << w[l]<< endl;
      }
      myfile2.close();
      return 0;
}
```

Appendix D: LED Info

IHEP Blue LED; Peak at 430 nm, spectral wavelength width 150nm. Pulse time width; tail after initial pulse up to 2μs for high energy pulses.

Chicago Miniature Blue LED; Peak at 470nm, spectral wavelength width 100nm. Pulse time width; 13ns, no tail end after initial pulse.

NICHIA UV; Peak at 315nm and 375nm, spectral wavelength width 50nm for each peak. Pulse time width; 20ns, slight tail end after initial pulse.

NICHIA UV; Peak at 365nm, spectral wavelength width 70nm. Pulse time width; unknown.

Red LED; Peak at 565nm and 645nm, spectral wavelength width 50nm and 90nm respectively. Pulse time width; tail end after initial pulse of approx. 1μs after initial pulse

Green LED; Peak at 560nm, spectral wavelength width 100nm. Pulse time width; 13ns, no tail end after initial pulse.

References:

[1]W. Pauli, Letter sent to the Tubingen conference, December 4th, 1930

[2]F. Reines and C. L. Cowan, Phys. Rev. 113 (1959) 273

[3]G. Danby et al. [Coumbia U. and Brookhaven], Phys. Rev. Lett. 9, 36 (1962)

[4]J. Bahcall and R. Davis Jr., On the Problem of Detecting Solar Neutrinos. BNL-8217 (1964)

[5]K. Kodama et al. [DONuT Collaboration], Physical Review D78 (2008)

[6]S. P. Mikheev and A. Y. Smirnov, Sov. J. Nucl. Phys. 42, 913 (1985); S. P. Mikheev and A. Y. Smirnov, Nuovo Cim. C 9, 17 (1986)

[7]L. Wolfenstein, Phys. Rev. D 17, 2369 (1978); L. Wolfenstein, Phys. Rev. D 20, 2634 (1979)

[8]K. S. Hirata et al. [Kamiokande-II Collaboration], Phys. Rev. Lett. 65, 1297 (1990); K. S. Hirata et al. [Kamiokande-II Collaboration], Phys. Rev. Lett. 65, 1301 (1990)

[9]Y. Fukuda et al. [Super Kamiokande Collaboration], Phys. Rev. Lett. 81, 1562 (1998)

[10]Q. R. Ahmad et al. [SNO Collaboration], Phys. Rev. Lett. 89, 011301 (2002)

[11]D. G. Michael et al. [Minos Collaboration], arXiv:hep-ex/0607088

[12]M. H. Ahn et al. [K2K Collaboration], Phys. Rev. Lett. B 28, 493 (1969)

[13]M. Apollonio et al. [Chooz Collaboration], Eur. Phys. J.C27, 331 (2003)

[14]Xinheng Guo et al. [Daya Bay Collaboration], Technical Design Report. (2008)

[15]Z. Maki, M. Nakagawa and S. Sakata, Prog. Theor. Phys. 28 870 (1962); B. Pontecorvo, Sov. Phys. JETP 26, 984 (1968); V. N. Gribov and B. Pontecorvo, Phys. Lett. 28B, 493 (1969)

[16][ATLAS Collaboration], Technical Design Report (1999)

[17]J. V. Jelley, Cerenkov Radiation and its Applications. New York, Pergamot Press (1958)

[18]W. R. Leo, Techniques for Nuclear and Particle Physics Experiments. New York, Springer (1994)

[19]E. Shibamura et al., Jap. Journal of App. Phys. Vol. 45, No. 7, 5990 (2006)

[20]D. Mohapatra, LED Calibration System for Water Pool LEDs. DYB-doc-2317-v1 (2008)

[21]Directed Energy, Inc., PCO-7110 Laser Diode Driver Module. Doc#9100-0214 Rev 4 (2000)
[22]J. Link, The Spectrum of Photons Seen by PMT (2008)
[23]Nichia Corporation, Specifications for Nichia UV LED Model: NSHU590A Cat. No. 081104
[24] Nichia Corporation, Specifications for Nichia UV LED Model: NSHU590B Cat. No. 081104